nature geoscience

ARTICLES

https://doi.org/10.1038/s41561-020-0561-x

Dry late accretion inferred from Venus's coupled atmosphere and internal evolution

C. Gillmann[1]✉, G. J. Golabek[2], S. N. Raymond[3], M. Schönbächler[4], P. J. Tackley[4], V. Dehant[5,6] and V. Debaille[1]

It remains contentious whether the meteoritic material delivered to the terrestrial planets after the end of core formation was rich or poor in water and other volatiles. As Venus's atmosphere has probably experienced less volatile recycling over its history than Earth's, it may be possible to constrain the volatile delivery to the primitive Venusian atmosphere from the planet's present-day atmospheric composition. Here we investigate the long-term evolution of Venus using self-consistent numerical simulations of global thermochemical mantle convection coupled with both an atmospheric evolution model and a late accretion N-body delivery model. We found that atmospheric escape is only able to remove a limited amount of water over the history of the planet, and that the late accretion of wet material exceeds this sink and would result in a present-day atmosphere that is too rich in volatiles. A preferentially dry composition of the late accretion impactors is most consistent with measurements of atmospheric H_2O, CO_2 and N_2. Hence, we suggest that the late accreted material delivered to Venus was mostly dry enstatite chondrite, consistent with isotopic data for Earth, with less than 2.5% (by mass) wet carbonaceous chondrites. In this scenario, the majority of Venus's and Earth's water would have been delivered during the main accretion phase.

The volatile inventory of terrestrial planets is of prime importance because it not only affects the atmosphere, surface conditions and potential habitability, but also influences mantle dynamics, the tectonic regime and volcanic outgassing[1,2]. Uncertainties remain mostly due to the limited data on the early volatile reservoirs[3] and to uncertain delivery scenarios[3–5].

After core formation ceased, late meteoritic material delivery occurred on Earth, which contributed as a late accretion (LA) an additional ≈0.5–1.5% of Earth's mass[5–7]. Although advances have been made to constrain Earth's LA, the exact nature of that late material remains debated when it comes to other bodies. It must account for the abundances of highly siderophile elements in the Earth's mantle, but might also have contributed to water delivery to the Earth[8]. Although volatile-rich bodies, such as carbonaceous chondrites (CCs), have been considered as ideal candidates, especially if the Earth's mantle was left dry after the Moon-forming giant impact[8], recent geochemical results argue for a LA on Earth that was mainly composed of dry material[9], such as enstatite chondrites (EC)[10].

Numerical results show that LA also occurred on Venus[11], but in the absence of samples from Venus, isotopic studies are limited to the planet's atmosphere[1,2,12]. Venus's past is poorly constrained; however, it was suggested that Venus experienced a more straightforward evolution of its volatile inventory[1,13]. Such an evolution would involve less volatile recycling, as Venus shows no sign of a biosphere, standing water or global plate tectonics.

Although it has been suggested that, under specific conditions, liquid water was stable on Venus for long periods of time[14], without a magma ocean there is no sufficiently strong oxygen sink to remove the oxygen that results from the eventual evaporation of a large water ocean caused by a runaway greenhouse effect[1,15,16]. Conversely, conditions during the global magma ocean phase are not compatible with the condensation of large bodies of water at the surface[1,17]: the condensation of water means the loss of the magma ocean and so the loss of the strongest oxygen sink. Thus, large bodies of liquid water are difficult to accommodate on Venus both early and late during its evolution. It is therefore likely that Venus has been desiccated since its early evolution[18], the extent and timing of which are still poorly constrained, and the recent surface conditions do not allow for water condensation and associated enhanced weathering[1,17].

Venus's massive CO_2 atmosphere also contains about as much CO_2 as all the atmospheric, crustal and mantle reservoirs on Earth. Thus, the present-day atmosphere of Venus is closer to its primitive inventory of CO_2, whereas on Earth, a comparable amount has been incorporated into carbonates and the mantle[1]. Without volatile recycling, Venus is also less likely to develop Earth-like plate tectonics[19], which explains the lack of a magnetic dynamo[20].

We propose a quantitative self-consistent model of Venus, focussing on the evolution of its volatile inventory since the LA. We combined N-body LA calculations[11] with a state-of-the-art coupled planet interior and atmospheric evolution model[21]. We modelled the consequences of LA on Venus's volatile history and the exchanges of three species (H_2O, CO_2 and N_2) between the planetary interior and atmosphere.

The early evolution of Venus

The evolution of Venus starts with its accretion, when the bulk of the mass of the planet is delivered[1]. Both accretionary impacts and the atmosphere result in temperatures high enough to create a magma ocean[22]. Owing to hydrodynamic escape, the primordial atmosphere thins over a timescale of a few tens of million years[12,15]. For a slow-to-moderate solar rotation period, modelling work on the isotopic fractionation of noble gases indicates the loss of a terrestrial water ocean every 10^5–10^7 years. Models also suggest that the magma ocean solidifies rapidly over a period of ≈1 Myr[17], when the atmospheric water content becomes small[17,18] due to hydrodynamic escape. The mantle enters the phase of solid-state convection

[1]Laboratoire G-Time, Université Libre de Bruxelles, Brussels, Belgium. [2]Bayerisches Geoinstitut, University of Bayreuth, Bayreuth, Germany. [3]Laboratoire d'Astrophysique de Bordeaux, CNRS and Université de Bordeaux, Pessac, France. [4]Department of Earth Sciences, ETH Zurich, Zurich, Switzerland. [5]Université catholique de Louvain, Louvain-la-Neuve, Belgium. [6]Royal Observatory of Belgium, Brussels, Belgium. ✉e-mail: cgillman@ulb.ac.be

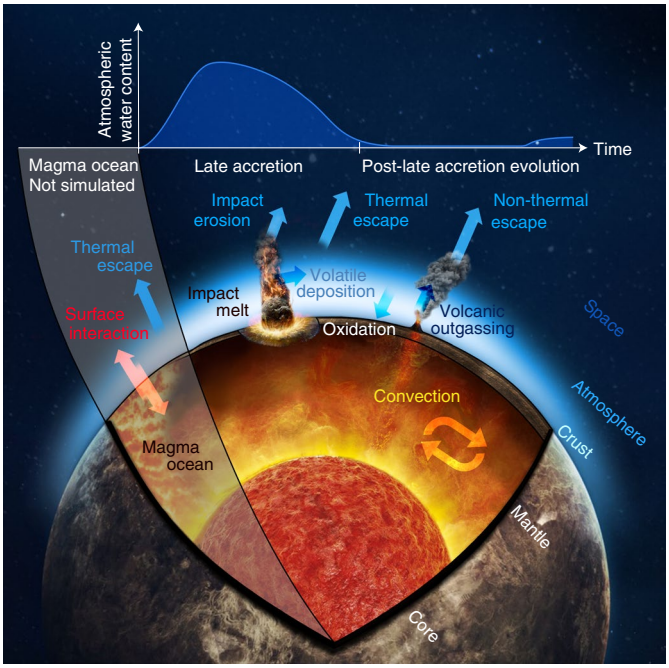

Fig. 1 | Volatile exchanges on Venus. Mechanisms that affect the water content of Venus's atmosphere during the long-term evolution of the planet.

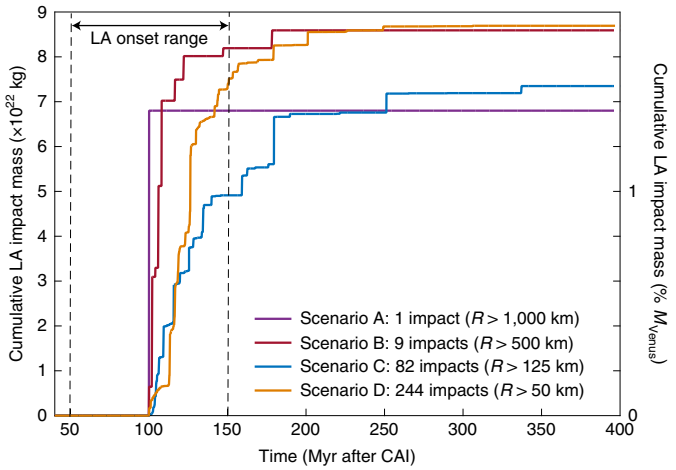

Fig. 2 | LA scenarios. Four distinct LA impact scenarios were used in the coupled interior-atmosphere models assuming a LA that began at 100 Myr after the formation of the CAIs. The considered variation in the LA onset time is shown by the dashed line box. The total mass of Venus LA was found to be larger than Earth's by a factor of 2–3. M_{Venus}, mass of Venus.

(Fig. 1), which we model here. Afterwards, LA delivers the final part of the planetary mass via impacts[5,6].

LA impacts have three main effects (all considered here): delivery of volatiles to the planet[8], impact heating[23] and erosion of the atmosphere[24]. We use N-body simulations to study LA, with various simulated growth histories that are consistent with the masses of present-day terrestrial planets. As it is possible that the size and number of impactors have consequences for the evolution, we tested four distinct LA impact scenarios (Fig. 2). These represent median cases based on several hundred N-body simulations[11]: a single very large impact (Scenario A, $R = 1{,}819$ km) (ref. [25]), 9 large impacts (Scenario B, $R > 500$ km), 82 medium-sized collisions (Scenario C, $R > 125$ km) and, finally, 244 small impactors (Scenario D, $R > 50$ km). However, we note that, given the top-heavy nature of the impacting size distributions, the mass tends to be dominated by the few largest bodies. The timing of LA on Venus is still debated, and thus onset times that range from 50 to 150 Myr (ref. [26]) after the formation of Ca–Al-rich inclusions (CAIs) are used, marking the start of the evolution models. Impactors have either an EC-like composition[27,28] (0.1% H_2O, 0.4% CO_2 and 0.02% N_2) or a CC composition[29,30] (8% H_2O, 4% CO_2 and 0.2% N_2), which thus determines the amount of volatiles delivered by LA to the atmosphere of Venus[31]. Intermediate ordinary chondrite (OC) compositions are also considered (Supplementary Information).

The consequences of volatile delivery

During the LA volatile delivery, strong escape mechanisms limit the accumulation of volatiles in the atmosphere. Thermal (hydrodynamic) escape dominates[12] the early evolution. As atmospheric water is photodissociated, the early hydrodynamic escape removes H_2 efficiently during the first few 100 Myr. As the removal of oxygen[1,12,32,33] by hydrodynamic escape is inefficient, it accumulates in the early atmosphere. However, the present-day atmosphere of Venus displays very little water or oxygen. Therefore, it must have been lost during the planetary evolution[1]. During the main accretion stage, oxidation of the molten magma ocean can trap oxygen efficiently[1,15,34], but from the LA stage onwards this sink only exists in the form of oxidation of the newly emplaced lava flows[35] and thus its consequences on oxygen removal are limited (Supplementary Information).

Non-thermal escape removes less mass than hydrodynamic escape does. However, it removes oxygen and affects the long-term evolution of the atmosphere. The balance between oxygen left in the atmosphere by LA, hydrodynamic escape and the long-term sink of non-thermal escape (plus putative oxidation mechanisms[34]), defines the upper limit of the LA volatile delivery and its composition.

As the removal of oxygen occurs on the timescale of billions of years, the entire evolution of Venus starting with LA needs consideration. To this end, the LA impact scenarios are incorporated into coupled atmosphere–interior evolution models that follow the model layout of Gillmann et al.[21] with volcanic outgassing considered as an additional volatile source (Methods). We modelled the evolution of the atmospheric volatile inventory starting after the end of the magma ocean stage until present-day. Comparison between the final state of the simulated atmosphere and the present-day atmosphere composition enabled us to constrain the volatile content of the LA material.

Our main constraint is the bulk composition of the present-day atmosphere of Venus, which is well-established[1], with 11×10^{18} kg of N_2 (2 bar[36]), 10^{16} kg of H_2O (2×10^{-3} bar[34,37]) and 4.69×10^{20} kg of CO_2 (90.6 bar[38]) (Methods). Other major constraints available to narrow down Venus evolution scenarios are the noble gas isotopic ratios and the D/H ratio. Noble gas isotopic ratios ($^{36}Ar/^{38}Ar$ and $^{20}Ne/^{22}Ne$) are thought to indicate that an early thermal escape fractionated these species[1,12]. However, this constraint on escape is weak, because it has been shown that no single solution meets the $^{36}Ar/^{38}Ar$ and $^{20}Ne/^{22}Ne$ fractionation[12]. We still used this constraint to assess the hydrodynamic escape fluxes. The upcoming Venera D mission may improve the noble gas isotopic measurements and provide tighter constraints on Venus's evolution. The D/H atmospheric ratio shows an enrichment of deuterium relative to that of Earth by a factor 100, which indicates water loss from the Venus atmosphere[39]. It is governed by a long-term non-thermal escape and its interaction with volcanic degassing sources of unknown composition[40], with additional effects from hydrodynamic escape[41] and impacts[42]. Moreover, measurements show that the D/H ratio in the atmosphere of Venus changes with altitude[39], which limits its value as a constraint. Thus, modelling of the D/H ratio evolution is not feasible here.

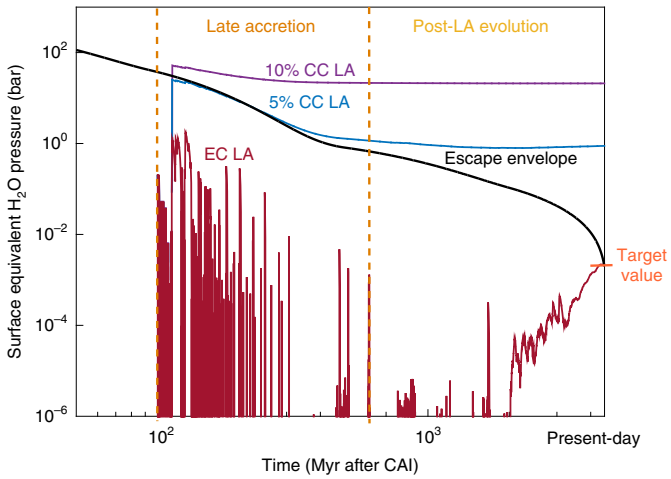

Fig. 3 | Evolution of water in the atmosphere of Venus. Time evolution of H_2O in the Venus atmosphere for MAX conditions assuming different LA compositions, labelled as CC material percentage of the total LA mass delivery. The LA scenario D that starts at 100 Myr after CAI formation is used.

Estimating the maximum LA delivery

At the start of the evolution model, after the magma ocean has solidified, the initial water content of Venus's atmosphere is assumed to have been completely removed during earlier evolution[1]. As our aim is to estimate the maximum volatile content of the LA, we chose the ideal initial conditions with no pre-existing water. Any oxygen that remained at the onset of the simulation also needs to be extracted from the atmosphere by the limited existing volatile sinks. This implies a reduced LA volatile delivery and reinforces our results. An early CO_2 atmosphere exists due to the magma-ocean outgassing, whereas N_2 is mostly trapped at the hot surface[43]. The initial volatile pressures at the start of the LA were chosen to be 0 bar N_2[43] and H_2O, and 65 bar CO_2[15]. CO_2 degassing of the magma ocean is considered to be efficient due to its low solubility in magma, and a thick CO_2 atmosphere forms early on[1,17]. The LA stage is characterized by volatile delivery due to impacts and subsequent volatile loss. Water delivery is dominated by impactors with a CC composition (if present) because of their high water content, whereas N_2 and CO_2 are deposited in large amounts by both CC and EC. Impact erosion effects[44] are noticeable but insufficient to prevent volatile build-up. Volcanic outgassing, which includes that caused by impact melting, also remains a second-order effect. The late evolution of atmospheric water content (from the end of the LA to present-day) is dominated by atmospheric escape and volcanic degassing, which also causes the slow accumulation of N_2 and CO_2 in Venus's atmosphere.

The major factor that limits H_2O evolution models is the 'escape envelope', which corresponds to the maximum amount of oxygen that can be removed by atmospheric escape between a given time and present-day[45] (Fig. 3a). It is obtained by cumulating losses based only on non-thermal escape processes from present-day, back to any given time in the past[46]. Thus, models in which the delivered water and consequent H_2O equivalent pressures exceed the escape envelope are not able to lose sufficient amounts of volatiles to meet present-day observations and are rejected. All the models are evaluated against the present-day volatile content of the atmosphere. As an additional constraint, Venus must lose all molecular oxygen that it accumulated during its early evolution due to hydrodynamic escape[1,46,47].

The evolution of water abundances shown in Fig. 3 represents an equivalent water concentration based on the fluxes of O atoms from both water delivery and losses. For H_2O, two distinct cases arise: either (1) H_2O is removed, the atmosphere desiccates and only limited volcanic degassing during late evolution replenishes it or (2) it remains in the atmosphere, which results in higher equivalent water pressures (>1 bar) for the rest of the evolution, which does not fit present-day observations of Venus. For CO_2 and N_2 the progression from one scenario to the other is much smoother (Extended Data Fig. 1).

The choice of non-thermal escape parameters is therefore crucial. Three main sets, which controlled the magnitude of volatile loss, were tested. The parameter set that allows the largest potential volatile deposition from the LA (that is, the most favourable to wet LA) was therefore considered as the upper limit for LA volatile content, and is denoted MAX. This end member is characterized by the maximum atmospheric escape[46], minimal outgassing[21] and the use of the tangent plane model for the impact-induced atmospheric erosion[44]. The parameter set called MIN causes the smallest loss and therefore the driest LA and is considered to be the most realistic[1]. A third scenario with intermediate volatile loss is called MED. Extended Data Figs. 2 and Fig. 3 show the evolution with the MED and MIN parameters.

Figure 4a,b shows the relative agreement between the model results and observations using the relative accuracy of simulations ($\alpha = 1 - |M_{S,i} - M_{obs,i}|/M_{obs,i}$, where i denotes the volatile species considered, and M_s and M_{obs} are the simulated and observed masses, respectively). Figure 4 summarizes the model results based on different LA onset times (Fig. 4a) and the four LA impact scenarios (Fig. 4b) for the cases that allow for a maximum volatile concentration in LA bodies. For comparison, Fig. 4c shows results for selected models using more realistic water losses. Based on H_2O only, the calculations show that a maximum of 2.5% of wet LA material consistently satisfies present-day conditions for a LA that began around 60–120 Myr after CAI formation (Fig. 4a). This is the equivalent of a single CC impactor ≈500 km in radius. The onset time of LA greatly affects the results in MAX cases, due to the additional losses it allows for. Late LA onsets (>150 Myr after CAI formation) are unlikely to fit the atmosphere composition data. Assuming an earlier LA onset (while keeping the same LA mass), the results for water imply a viable amount of up to 10–15% of wet LA material. However, N_2 and CO_2 evolution provide additional constraints, as their loss rates are lower than those of water[1,46]. Correspondingly, early volatile-rich LA models that satisfy the H_2O content are unable to simultaneously meet present-day N_2 and CO_2 measurements. In the case of LA that contains 10% CC material, the present-day amount of CO_2 is 22% off (≈20 bars), whereas N_2 is 40% off (≈0.7 bar). These discrepancies are larger than the total contribution of volcanic outgassing for CO_2 and N_2, respectively (Extended Data Fig. 4). Therefore, such a LA composition is in disagreement with the measured atmospheric composition data, and the excess of volatiles cannot be attributed to excessive outgassing. Therefore, the maximum contribution of CC in LA is <2.5% for LA onset times >100 Myr after CAI formation and <10% for earlier LA onsets. Thus, our results do not allow us to constrain the LA onset time on Venus, but rather, indirectly, the impact time of the last major wet impactor[45].

Figure 4b illustrates the interplay of total LA mass and the number of impactors. Larger masses result in more volatile delivery. However, for a given mass, many small impacts cause more atmospheric erosion than a smaller number of larger impactors. Thus, Fig. 4b implies that the size-frequency distribution of LA impactors has only minor effects on our conclusions, especially for water. In particular, we do not expect our results to change if the LA impactors had a size distribution that was less top-heavy and closer to the present-day asteroid size distribution. Figure 4c shows water-loss estimates based on the MIN parameter, which represent more accurately our current understanding of solar extreme ultraviolet (EUV) and water-loss evolution[1]. MIN models are extremely restrictive and have a tighter limit on water delivery. The escape envelope shows a small slope, and thus is not able to constrain the LA onset time very well. This parameter set requires a dry LA scenario, with less than

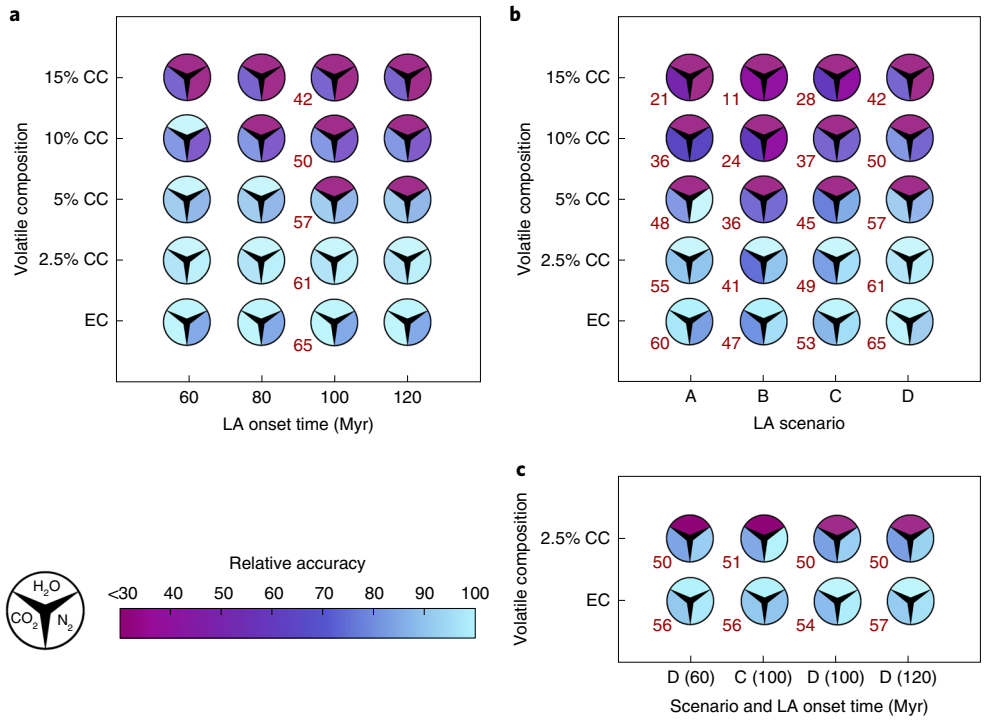

Fig. 4 | Consequences of LA volatile content on present-day Venus atmosphere. a–c, Agreement (relative accuracy) between the model results and the present-day volatile content of Venus's atmosphere assuming a strong atmospheric escape (MAX parameter set) (**a**,**b**) and using a weak atmospheric escape (MIN parameter set) (**c**). **a**, Scenario D starting at 60–120 Myr after CAI and different LA compositions that range from an EC end member to 15% of the CC material. **b**, LA scenarios A–D with LA onset at 100 Myr after CAI and assuming the same variation of LA compositions as in **a**. **c**, Selection of simulations that employ scenarios C and D with different LA onset times. EC composition simulations display a deficit in N_2 relative to present-day atmospheric content. Red numbers indicate the post-magma ocean CO_2 pressure (bar) required as the initial condition to increase the CO_2 agreement at present-day to 100%. The perceptually uniform colour map is reproduced from ref. [51], EGU, StagLab 3.0, under a CC BY 4.0 licence.

2.5% CC (and >97.5% EC material), regardless of the LA onset time and implies that impactors may have been substantially desiccated[48].

In conclusion, the best fit between models and present-day Venus atmosphere shows that the LA on Venus was primarily composed of EC-like (dry) meteorites with at most 2.5% of the total mass exhibiting a CC (wet) composition. Venus and its atmosphere have therefore not received any major volatile deliveries after the end of the magma ocean. Numerical models suggest that the LA could have been homogeneous in the early solar system with comparable compositions, which include that for water[11,13,49]. In this case, our conclusions agree with previous suggestions based on isotopic studies for both Earth and Mars material[9,10,50] and indicate that the majority of volatiles was delivered to the terrestrial planets during planet formation, and thus, in the case of Earth, before the Moon-forming giant impact.

Online content

Any methods, additional references, Nature Research reporting summaries, source data, extended data, supplementary information, acknowledgements, peer review information; details of author contributions and competing interests; and statements of data and code availability are available at https://doi.org/10.1038/s41561-020-0561-x.

Received: 21 March 2019; Accepted: 26 February 2020;
Published online: 07 April 2020

References

1. Lammer, H. et al. Origin and evolution of the atmospheres of early Venus, Earth and Mars. *Astron. Astrophys. Rev.* **26**, 2 (2018).
2. Lammer, H. et al. What makes a planet habitable? *Astron. Astrophys. Rev.* **17**, 181–249 (2009).
3. Raymond, S. N. & Izidoro, A. Origin of water in the inner Solar System: planetesimals scattered inward during Jupiter and Saturn's rapid gas accretion. *Icarus* **297**, 134–148 (2017).
4. O'Brien, D. P., Izidoro, A., Jacobson, S. A., Raymond, S. N. & Rubie, D. C. The delivery of water during terrestrial planet formation. *Space Sci. Rev.* **214**, 47 (2018).
5. Morbidelli, A. & Wood, B. J. in *The Early Earth: Accretion and Differentiation* (eds Badro, J. & Walter, M. J.) 71–82 (Geophysical Monograph Series Vol. 212, American Geophysical Union, 2015).
6. Rubie, D. C. et al. Highly siderophile elements were stripped from Earth's mantle by iron sulfide segregation. *Science* **353**, 1141–1144 (2016).
7. Day, J. M., Pearson, D. G. & Taylor, L. A. Highly siderophile element constraints on accretion and differentiation of the Earth–Moon system. *Science* **315**, 217–219 (2007).
8. Albarède, F. Volatile accretion history of the terrestrial planets and dynamic implications. *Nature* **461**, 1227–1233 (2009).
9. Fischer-Gödde, M. & Kleine, T. Ruthenium isotopic evidence for an inner Solar System origin of the late veneer. *Nature* **541**, 525–527 (2017).
10. Dauphas, N. The isotopic nature of the Earth's accreting material through time. *Nature* **541**, 521–524 (2017).
11. Raymond, S. N., Schlichting, H. E., Hersant, F. & Selsis, F. Dynamical and collisional constraints on a stochastic late veneer on the terrestrial planets. *Icarus* **226**, 671–681 (2013).
12. Odert, P. et al. Escape and fractionation of volatiles and noble gases from Mars-sized planetary embryos and growing protoplanets. *Icarus* **307**, 327–346 (2018).
13. Peslier, A. H., Schönbächler, M., Busemann, H. & Karato, S. I. Water in the Earth's interior: distribution and origin. *Space Sci. Rev.* **212**, 743–810 (2017).
14. Way, M. J. et al. Was Venus the first habitable world of our solar system? *Geophys. Res. Lett.* **43**, 8376–8383 (2016).
15. Lichtenegger, H. I. M. et al. Solar XUV and ENA-driven water loss from early Venus' steam atmosphere. *J. Geophys. Res.* **121**, 4718–4732 (2016).

16. Rasool, S. I. & de Bergh, C. The runaway greenhouse effect and the accumulation of CO_2 in the atmosphere of Venus. *Nature* **226**, 1037–1039 (1970).
17. Salvador, A. et al. The relative influence of H_2O and CO_2 on the primitive surface conditions and evolution of rocky planets. *J. Geophys. Res.* **122**, 1458–1486 (2017).
18. Hamano, K., Abe, Y. & Genda, H. Emergence of two types of terrestrial planet on solidification of magma ocean. *Nature* **497**, 607–610 (2013).
19. Solomatov, V. S. Initiation of subduction by small-scale convection. *J. Geophys. Res.* **109**, B01412 (2004).
20. Driscoll, P. & Bercovici, D. Divergent evolution of Earth and Venus: influence of degassing, tectonics, and magnetic fields. *Icarus* **226**, 1447–1464 (2013).
21. Gillmann, C., Golabek, G. J. & Tackley, P. J. Effect of a single large impact on the coupled atmosphere–interior evolution of Venus. *Icarus* **268**, 295–312 (2016).
22. Elkins-Tanton, L. T. Magma oceans in the inner solar system. *Annu. Rev. Earth Planet. Sci.* **40**, 113–139 (2012).
23. Monteux, J. et al. Mechanical adjustment after impacts during planetary growth. *Geophys. Res. Lett.* **34**, L24201 (2007).
24. Shuvalov, V. Atmospheric erosion induced by oblique impacts. *Meteorit. Planet. Sci.* **44**, 1095–1105 (2009).
25. Brasser, R., Mojzsis, S. J., Werner, S. C., Matsumura, S. & Ida, S. Late veneer and late accretion to the terrestrial planets. *Earth Planet. Sci. Lett.* **455**, 85–93 (2016).
26. Jacobson, S. A. et al. Highly siderophile elements in Earth's mantle as a clock for the Moon-forming impact. *Nature* **508**, 84–87 (2014).
27. Pepin, R. O. On the origin and early evolution of terrestrial planet atmospheres and meteoritic volatiles. *Icarus* **92**, 2–79 (1991).
28. Muenow, D. W. & Wilson, L. High-temperature mass spectrometric degassing of enstatite chondrites: implications for pyroclastic volcanism on the aubrite parent body. *Geochim. Cosmochim. Acta* **56**, 4267–4280 (1992).
29. Marty, B. The origins and concentrations of water, carbon, nitrogen and noble gases on Earth. *Earth Planet. Sci. Lett.* **313**, 56–66 (2012).
30. Pearson, V. K. et al. Carbon and nitrogen in carbonaceous chondrites: elemental abundances and stable isotopic compositions. *Meteorit. Planet. Sci.* **41**, 1899–1918 (2006).
31. Sakuraba, H., Kurokawa, H. & Genda, H. Impact degassing and atmospheric erosion on Venus, Earth, and Mars during the late accretion. *Icarus* **317**, 48–58 (2019).
32. Schaefer, L., Wordsworth, R. D., Berta-Thompson, Z. & Sasselov, D. Predictions of the atmospheric composition of GJ 1132b. *Astrophys. J.* **829**, 63 (2016).
33. Zahnle, K. J. & Kasting, J. F. Mass fractionation during transonic escape and implications for loss of water from Mars and Venus. *Icarus* **68**, 462–480 (1986).
34. Kasting, J. F. & Pollack, J. B. Loss of water from Venus. I. Hydrodynamic escape of hydrogen. *Icarus* **53**, 479–508 (1983).
35. Filiberto, J., Trang, D., Treiman, A. H. & Gilmore, M. S. Present-day volcanism on Venus as evidenced from weathering rates of olivine. *Sci. Adv.* **6**, eaax7445 (2020).
36. Johnson, B. & Goldblatt, C. The nitrogen budget of Earth. *Earth-Sci. Rev.* **148**, 150–173 (2015).
37. Lécuyer, C., Simon, L. & Guyot, F. Comparison of carbon, nitrogen and water budgets on Venus and the Earth. *Earth Planet. Sci. Lett.* **181**, 33–40 (2000).
38. Fegley. B. Jr in *Planets, Asteroids, Comets, and the Solar System* 2nd edn (eds Holland, H. D. & Turekian, K. K.) 127–148 (Treatise on Geochemistry, Vol. 2, Elsevier, 2014).
39. Marcq, E., Mills, F. P., Parkinson, C. D. & Vandaele, A. C. Composition and chemistry of the neutral atmosphere of Venus. *Space Sci. Rev.* **214**, 10 (2018).
40. Grinspoon, D. H. Implications of the high D/H ratio for the sources of water in Venus' atmosphere. *Nature* **363**, 428–431 (1993).
41. Kasting, J. F., Pollack, J. B. & Ackerman, T. P. Response of Earth's atmosphere to increases in solar flux and implications for loss of water from Venus. *Icarus* **57**, 335–355 (1984).
42. Zahnle, K. J. in *Protostars and Planets III* (eds Levy, E. H. & Lunine, J. I.) 1305–1338 (Univ. Arizona Press, 1993).
43. Wordsworth, R. D. Atmospheric nitrogen evolution on Earth and Venus. *Earth Planet. Sci. Lett.* **447**, 103–111 (2016).
44. Melosh, H. J. & Vickery, A. M. Impact erosion of the primordial atmosphere of Mars. *Nature* **338**, 487–489 (1989).
45. Griffith, C. A. & Zahnle, K. Influx of cometary volatiles to planetary moons: the atmospheres of 1000 possible Titans. *J. Geophys. Res. Planet.* **100**, 16907–16922 (1995).
46. Kulikov, Y. N. et al. Atmospheric and water loss from early Venus. *Planet. Space Sci.* **54**, 1425–1444 (2006).
47. Gillmann, C., Chassefière, E. & Lognonné, P. A consistent picture of early hydrodynamic escape of Venus atmosphere explaining present Ne and Ar isotopic ratios and low oxygen atmospheric content. *Earth Planet. Sci. Lett.* **286**, 503–513 (2009).
48. Lichtenberg, T. et al. A water budget dichotomy of rocky protoplanets from ^{26}Al-heating. *Nat. Astron.* **2**, 307–313 (2019).
49. Rubie, D. C. et al. Accretion and differentiation of the terrestrial planets with implications for the compositions of early-formed Solar System bodies and accretion of water. *Icarus* **248**, 89–108 (2015).
50. Schönbächler, M., Carlson, R. W., Horan, M. F., Mock, T. D. & Hauri, E. H. Heterogeneous accretion and the moderately volatile element budget of Earth. *Science* **328**, 884–887 (2010).
51. Crameri, F. Geodynamic diagnostics, scientific visualisation and StagLab 3.0. *Geosci. Model Dev.* **11**, 2541–2562 (2018).

Methods

The coupled atmosphere–interior model considers four main aspects that define the long-term evolution of Venus: (1) volcanic degassing of volatiles, (2) atmosphere escape sinks, (3) surface condition evolution and (4) LA impacts. We tested three distinct parameter sets: MAX parameters (which allow for a maximum LA volatile contribution; see main text), MED parameters (average parameter; Supplementary Information) and MIN parameters (which allow for a minimum LA volatile contribution; see main text). Extended Data Figs. 5 and 6 give more details and the list of models is given in Supplemental Table 1. Based on present-day knowledge, the MIN parameter set is considered to be the most realistic[5]. The MAX parameter set leads to extreme escape cases; it is used for the numerical models discussed in the main text because the extreme nature of this parameter set also ensures that results are robust to parameter variations. All the atmospheric volatile pressures are expressed assuming that this specific gas is the only one in the atmosphere, and are therefore a proxy of mass. As a reference, one terrestrial ocean corresponds to 265 bar, 1.39×10^{21} kg and a global equivalent layer of 2,900 m depth.

Numerical modelling of thermochemical convection. We modelled the mantle dynamics for a 4.5 Gyr period, from the end of the magma ocean stage until the present-day. We used the version of the code StagYY[52] described in Armann and Tackley[53], Gillmann and Tackley[54] and Gillmann et al.[21]. The tectonic regime of the planet is not prescribed, but it is calculated self-consistently. In the present simulations Venus does not exhibit Earth-like plate tectonics. Supplementary Annex 1 contains a full description.

Melt eruption and volatile outgassing. Melt generated during the mantle convection and reaching the surface of Venus contributes to volatile outgassing of N_2, CO_2 and H_2O. The full description of the outgassing process and parameters can be found in Supplementary Annex 1. Extended Data Fig. 4 shows the impact and volcanic contributions.

Solar evolution. The long-term evolution of EUV flux from the Sun and solar wind affect atmospheric escape[15,46,55]. EUV flux decreases with time according to a power law[56], which assumes that the early Sun was a slow-to-moderate rotator, as suggested by recent studies[1,57]. Luminosity increases with time, according to the faint young Sun hypothesis[58,59] from 70% of present-day luminosity to the present-day value.

Hydrodynamic and thermal escape. Hydrodynamic and thermal escape describes the response of a primitive, hydrogen-rich atmosphere subjected to high-intensity EUV radiation. The atmosphere expands, hydrogen escapes and heavier species can be dragged along only for as long as the driving H flux persists. We used the energy-limited model of hydrogen escape described in Gillmann et al.[47] and based on previous work[33,34,60–63]. Maximum escape fluxes calculated for hydrogen are $\approx3\times10^{31}$ s^{-1}, consistent with estimates from recent work[15,46]. Photodissociation splits water molecules into H and O atoms. As H escape is much more efficient than O escape, hydrodynamic escape generates an accumulation of O (possibly as much as 85 bars O[62,63]) that needs to be removed from the atmosphere: only early on can it be stored in the magma ocean. At the onset of the model, all the primordial water is thus assumed to have been removed from the atmosphere[1]. Any oxygen remaining in the atmosphere reduces potential water delivery during the LA. Additionally, this means that most of the thermal escapes of oxygen and CO_2 occur during the magma ocean phase, before the onset of our model, and therefore controls the initial volatile inventory. CO_2 losses have been suggested to be low (<10 bar[15,46,64,65]). N_2 was protected due to the cooling effect of CO_2 in the upper atmosphere[1]. Later on, during and after the LA, oxygen and CO_2 are lost primarily by non-thermal escape mechanisms[1,46,47], due to the lack of a late long-lived hydrogen-rich atmosphere[1]. Therefore, owing to its very limited losses during and after the LA, CO_2 thermal escape rates are not considered in the model. The error between modelled and observed present-day CO_2 pressures was determined and a corrected initial pressure necessary to reduce the error to zero was calculated (Fig. 4).

Non-thermal escape. Non-thermal escape covers the interaction of upper atmosphere particles with the high-energy radiation from the Sun, such as, for example, the EUV flux. The mechanisms involved are photochemical reactions[66], sputtering[67], ion pick-up[68] and plasma instabilities[55]. Non-thermal escape dominates late evolution (3.5 billion years ago (Ga) to present), but also plays a role earlier on. We reconstructed past non-thermal escape fluxes in two stages: before and after 3 Ga, as detailed in the next two paragraphs. The cumulated effect of oxygen loss over time is shown as the escape envelope in Fig. 3. Non-thermal CO_2 losses are very small over the history of Venus[21,46].

Recent water loss. Recent water loss is calculated from O escape rates. Late evolution rates for the past 3 Gyr are calculated as in Gillmann et al.[21,54], based on simulations and present-day measurements[64] of atmospheric escape rates at solar minimum and solar maximum EUV conditions. An interpolation between those two values indicates how escape varies over a solar cycle, depending on the EUV flux. Solar maximum conditions of a present-day solar cycle correspond to the solar minimum EUV conditions 2.5–2.8 Ga[56]. Thus, we have access to the variation of escape rates for minimum solar conditions over the past 2.8 Gyr, which we extrapolate to mean escape rates used for the time period 0–3 Gyr before present-day. We used a cumulated present-day escape rate of 6×20^{25} s^{-1} (combining all O loss mechanisms), close to the maximum limit derived for present-day conditions[4]. The reconstruction is consistent with simulations from Kulikov et al.[46].

LA-era O excess removal. The early non-thermal escape was calculated using numerical simulations[46] of the ion-pick-up loss flux based on a particle model[69] and taking into account the stronger early solar activity (EUV about 100 times the present-day value 4.5 Ga[59]). Specifically, we used case 2b in Kulikov et al.[46] (moderate solar wind activity). This estimate corresponds to the effect of ion-pick-up only. The total escape, which accounts for all the mechanisms, is several times higher[64]. MAX (main text and figures) and MED (extended data) parameter cases use a multiplication factor of 5 and 2.5, respectively (case 2b in Kulikov et al.[46]), to account for higher and lower escape ranges. A low escape (case 4 in Kulikov et al.[46]), which represents recent advances in the characterization of solar evolution[1,70,71], is used in the MIN parameter cases. Further models use the lowest possible multiplicative factor (6) able to accommodate LA scenario D with the EC composition. Extended Data Fig. 6 compares parameters for these three cases. Although thermal escape remains unaffected by the presence of a magnetic field, non-thermal escape is affected. It is currently uncertain whether Venus had a magnetosphere in the past[72], and there is currently no sign of a present-day magnetosphere. It has been suggested that, if Venus exhibited Earth-like conditions, it would probably still maintain a magnetic field at the present-day[72]. However, if Venus had a stratified core, it would not have generated a magnetic field[73]. Given our present knowledge of the effects of magnetic fields, it is unknown whether the presence of a magnetosphere would result in decreased or increased atmospheric losses[74]. In case the atmosphere is shielded, our conclusions are reinforced. Assuming an end-member scenario in which Venus had a magnetosphere during its entire evolution, which results in the maximum additional H_2O losses[74], leads to an increased maximum contribution of CC material in our models of up to 15%, 10% and 3% assuming MAX, MED and MIN parameter sets, respectively. However, the N_2 and CO_2 limits remain unchanged (Fig. 4).

Surface oxidation sink. Oxidation of the surface of Venus has been proposed as a possible oxygen sink[34,41] and would be consistent with the suggestion[75] of an oxidized basaltic surface. We performed additional numerical calculations that include surface oxidation to assess its consequences on the results of the model. We considered the following chemical reaction[37]: $2FeSiO_3 + ½O_2 \rightarrow Fe_2O_3 + 2SiO_2$.

Freshly erupted lava is able to react with oxygen while it is still hot. However, as the diffusion of oxygen in hot lava is slow, the process is inefficient. Results of the simulations and a full description of the calculations are available in Supplementary Annex 1. The effect of oxidation is noticeable, but only a small amount of up to a few bars of oxygen at most is removed from the atmosphere in this way.

Surface conditions. Surface temperature is calculated using a one-dimensional (1D), vertical, radiative-convective grey atmosphere model, as described in Gillmann et al.[54]. The atmosphere is considered to be in hydrostatic equilibrium and in a regime similar to that of present-day. The equilibrium temperature of the planet evolves with solar luminosity. CO_2 and H_2O are the only greenhouse gases considered here. Over time, the CO_2 content of the atmosphere only varies moderately compared with those of present-day conditions. Water atmospheric concentration is more variable, but within the bounds of previously tested models[21,54]. The surface temperatures calculated were found to be consistent with canonical values[1]. Changes in surface temperature affect convection[54], but the consequences on the volatile repartition are marginal, due to the low outgassing efficiency. Simulations with a constant surface temperature show a 3% change in the atmospheric volatile inventory.

LA scenarios. We used a series of N-body simulations from Raymond et al.[11] to generate a population of impacting bodies for Venus's LA. These simulations provide plausible evolutionary histories that match our current interpretation of the constraints. In our simulations, Jupiter and Saturn were included on orbits consistent with their gas-driven orbital migration[76–78]. The terrestrial 'leftovers' were included on orbits consistent with simulations of terrestrial planet formation[79,80]: the orbital semi-major axis was randomly chosen between 0.5 and 1.7 au, the eccentricity between 0.1 and 0.6, and the inclination between 0 and 20°. The mass of the leftovers was drawn from a size distribution consistent with Bottke et al.[81] and parameterized as $dN/dD \sim D^{-q}$, where N is the number of objects of a given diameter D and q was chosen to be 1, 1.5 or 2. For the main set of simulations[11], terrestrial leftovers (minimum diameter of 1,000 km) represent a population totalling 5% of Earth's mass, which was found to deliver the correct amount of LA mass to Earth[11]. Scenarios A and B adopted the stochastic LA framework of Bottke et al.[81], who suggested that a top-heavy mass distribution could explain why Earth experienced a more substantial LA than that inferred for the Moon or Mars[7,82]. Owing to the limited number of impactors in scenarios

A and B, small number statistics has to be considered. For this purpose, these two scenarios employed median cases based on hundreds of N-body simulations from Raymond et al.[11]. We also considered LA scenarios that involved smaller impactors[83]. These higher-resolution simulations (scenarios C and D) use minimum diameters of 100 and 250 km. All the scenarios used here were found to deliver the correct amount of LA material to the Earth (0.25–0.75% of Earth's mass)[5–7], which satisfies the highly siderophile element constraints. As a rule, they deliver a slightly larger mass as for the LA to Venus. This is consistent with the findings of Jacobson et al.[26]. Our simulations start with fully formed terrestrial planets and a population of leftovers, which implies that 'time zero' for these simulations was the last giant impact on any of the terrestrial planets, (the Moon-forming impact, roughly 50–150 Myr after the CAI formation for Earth[84,85]). It has been shown that an early last giant impact on Venus implies a larger total LA mass of up to ≈20% of the planet's mass[26,73]. Such LA scenarios result in additional volatile delivery and are unlikely to accommodate CC material. We performed numerical calculations using a modified scenario D in which the LA onset is at 20 Myr after CAI formation and all impactor masses are scaled up, so the total LA mass is 10% of the Venus mass (Supplementary Table 1). The results indicate no more than 10% CC material is permitted to match the present-day H_2O atmospheric content, whereas N_2 and CO_2 deliveries do not match with present-day observations. We found the differences between models A to D to be small (Fig. 4), and mainly due to differences in total mass. This leads us to expect that the size distribution of the LA impactors is not a critical factor for atmospheric volatile content and that our model would still match the constraints for a different distribution more characteristic of those of the present-day asteroid belt.

LA composition. Two compositional end members were chosen: ECs[27,28] or CCs[29,30,86]. Reducing the water content of the EC end member does not affect the maximum mass of CC compatible with atmospheric constraints by more than 1%, because water delivery is dominated by the CC bodies. An EC H_2O concentration reduced by a factor ten has been tested without a notable change to the results (Supplementary Table 1). The effects of variations in CC water content are shown in Supplementary Information Table 1; our conclusions remain unaffected.

We performed several calculations with an OC end member instead of a CC composition[87,88], using 1% H_2O, 1% CO_2 and 0.01% N_2. Lower water concentrations make this reservoir very similar to the EC end member and the resulting evolutions are close to those of the EC-only cases featured in Supplementary Table 1. The results for the OC LA scenarios indicate a correspondingly higher fraction of the wet end member with less than 45% OC with the MAX, 30% with the MED and 10% with the MIN parameter sets. This is (especially for MED) in line with the results obtained by Brasser et al.[89].

In scenarios B–D, the compositional variation is handled by assigning part of the LA impactors up to the desired mass fraction CC composition, whereas the bulk of the impactors have an EC composition. Those impactors with a CC composition are always assumed to collide with Venus during the first 20 Myr of the specific LA scenario to maximize volatile loss. For control models and scenario A, all the impactors have a uniform intermediate composition. Control models (Supplementary Table 1) exhibit marginal changes, which indicates they can accommodate 1–3% (weight) more CC material.

Impact-induced atmosphere erosion. Impacts can cause atmospheric loss due to atmospheric entry, ejecta material and vapour plume generation. Here, we used two approaches to model impact erosion[21]: (1) the tangent plane model[44,90] and (2) results from SOVA hydrocode simulations[24,91,92]. The tangent plane model predicts the removal of all the atmospheric content above a plane tangent to the surface of the planet at the impact location, and thus each collision removes $\approx 10^{-3}$ times the mass of the atmosphere of Venus. We considered for the MAX and MED parameter models that all the LA impactors are large enough to cause atmospheric escape as described by the tangent plane model. The SOVA hydrocode results imply lower erosion rates and are used for MIN parameter models. For large bodies ($R > 100$ km), SOVA-derived erosion efficiencies are reduced by a factor of ≈4 compared to the tangent plane model. Here, the total amount of atmospheric erosion by a certain LA scenario is primarily dictated by the number of impacts. We neglected ground-motion atmospheric erosion[93], which may be important for large impacts (scenario A) but negligible for smaller ones (scenarios B–D). This mechanism would increase the impact erosion in scenario A and make it comparable to those of scenarios C and D, and thus lead to more uniform results across all mass-size distributions.

Impact delivery of volatiles. Volatile delivery depends on the impactor composition (see above) and the fraction of the volatiles released during the collision that remain in the atmosphere afterwards. This deposition efficiency must take into account the portion of impactor material retained and the outgassing of volatiles from the impactor material. Numerical simulations[24,91,94] suggest that a minor fraction (10%) of the projectile can be lost back to space as ejecta material. We considered that only vaporized impactor material contributed to the outgassing of volatiles. We used a conservative value for the vaporized fraction of 40%[94–96], which led to a deposition efficiency of 36%. In the case that a larger part of the projectile is vaporized, the conclusions presented in the main text are reinforced. We tested low-end deposition efficiency factors (12%; Supplementary Table 1) with similar conclusions that led to a maximum EC fraction of ≈10% for the MAX parameters (less than 5% for MED and 2.5% for MIN).

Impact heating. Shock heating generates a high-temperature region in the planetary interior. Mantle volume and temperature increase in this thermal anomaly were treated here as in Gillmann et al.[21,23], taking into account impact velocities higher than the escape velocity[11,97]. Only impactors large enough ($R > 150$ km) to penetrate the lithosphere[21,23] were considered to have an important effect on the temperature structure of the planet's convecting interior. Smaller impactors only contributed to the atmosphere's evolution. Crustal vaporization was neglected. Compared to 3D geometry, the 2D geometry introduces an overestimation of the relative mantle volume affected by thermal anomalies[21]. In 2D and 3D, the ratio of affected volume to mantle volume varies with $R^2_{\mathrm{anomaly}}/(R^2_{\mathrm{Venus}} - R^2_{\mathrm{core}})$ and $R^3_{\mathrm{anomaly}}/(R^3_{\mathrm{Venus}} - R^3_{\mathrm{core}})$, where R_{Venus}, R_{core} and R_{anomaly} are the radii of the planet, its core and the isobaric core of the thermal anomaly, respectively[98]. The ratio between these two values approximates the overestimation caused by geometry. For large impacts ($R > 500$ km), it is ≈3, whereas for medium-sized collisions ($150 \leq R \leq 500$ km) the factor is ≈7. Therefore, only one in three large impactors and one in seven medium-sized ones are considered to create a thermal anomaly.

Data availability

The data that support the findings reported in this article are available as follows: code outputs of N-body simulations (impactors and collisions parameters) are available from figshare, with the identifier https://doi.org/10.6084/m9.figshare.11829621. Data generated for the models displayed in the figures (equivalent pressure evolutions) are available from figshare, with the identifier https://doi.org/10.6084/m9.figshare.11829621. Datasets generated during the current study as the present-day Venus atmosphere composition for the full complement of models are available in Supplementary Information.

Code availability

The convection code StagYY is the property of P.J.T. and Eidgenössische Technische Hochschule (ETH) Zürich. It is available on request from P.J.T. (paul.tackley@erdw.ethz.ch). The N-body model MERCURY, used for the LA scenarios, is available at https://github.com/4xxi/mercury.

References

52. Tackley, P. J. Modelling compressible mantle convection with large viscosity contrasts in a three-dimensional spherical shell using the yin-yang grid. *Phys. Earth Planet. Int.* **171**, 7–18 (2008).
53. Armann, M. & Tackley, P. J. Simulating the thermochemical magmatic and tectonic evolution of Venus's mantle and lithosphere: two-dimensional models. *J. Geophys. Res.* **117**, E12003 (2012).
54. Gillmann, C. & Tackley, P. J. Atmosphere/mantle coupling and feedback on Venus. *J. Geophys. Res.* **119**, 1189–1217 (2014).
55. Lammer, H. et al. Loss of hydrogen and oxygen from the upper atmosphere of Venus. *Planet. Space Sci.* **54**, 1445–1456 (2006).
56. Ribas, I., Guinan, E. F., Güdel, M. & Audard, M. Evolution of the solar activity over time and effects on planetary atmospheres. I. High-energy irradiances (1–1700 Å). *Astrophys. J.* **622**, 680–694 (2005).
57. Saxena, P., Killen, R. M., Airapetian, V., Petro, N. E. & Mandell, A. The Sun was likely not a fast rotator: using lunar moderate volatile depletion and solar analogue activity from Kepler data as constraints. In *AGU Fall Meeting 2018* (session conveners Meyer, H. M. et al.) Abstract P23D-3479 (AGU, 2018).
58. Gough, D. O. Solar interior structure and luminosity variations. *Solar Phys.* **74**, 21–34 (1981).
59. Ribas, I. et al. Evolution of the solar activity over time and effects on planetary atmospheres. II. κ1 Ceti, an analog of the Sun when life arose on Earth. *Astrophys. J.* **714**, 384–395 (2010).
60. Hunten, D., Pepin, R. & Walker, J. Mass fractionation in hydrodynamic escape (of gases from planetary atmospheres). *Icarus* **69**, 532–549 (1987).
61. Chassefière, E. Hydrodynamic escape of oxygen from primitive atmospheres: applications to the cases of Venus and Mars. *Icarus* **124**, 537–552 (1996).
62. Chassefière, E. Hydrodynamic escape of hydrogen from a hot water-rich atmosphere: the case of Venus. *J. Geophys. Res.* **101**, 26039–26056 (1996).
63. Chassefière, E. Loss of water on the young Venus: the effect of a strong primitive solar wind. *Icarus* **126**, 229–232 (1997).
64. Lammer, H. et al. Atmospheric escape and evolution of terrestrial planets and satellites. *Space Sci. Rev.* **139**, 399–436 (2008).
65. Lammer, H. et al. Pathways to Earth-like atmospheres. *Orig. Life Evol. Biospheres* **41**, 503–522 (2011).
66. Fox, J. L. & Bakalian, F. M. Photochemical escape of atomic carbon from Mars. *J. Geophys. Res.* **106**, 28785–28795 (2001).
67. Chassefière, E. & Leblanc, F. Mars atmospheric escape and evolution; interaction with the solar wind. *Planet. Space Sci.* **52**, 1039–1058 (2004).

68. Lundin, R. & Barabash, S. Evolution of the Martian atmosphere and hydrosphere: solar wind erosion studied by ASPERA-3 on Mars Express. *Planet. Space Sci.* **52**, 1059–1071 (2004).
69. Spreiter, J. R. & Stahara, S. S. Solar wind flow past Venus: theory and comparisons. *J. Geophys. Res.* **98**, 17251–17262 (1980).
70. Johnstone, C. P. et al. The evolution of stellar rotation and the hydrogen atmospheres of habitable-zone terrestrial planets. *Astrophys. J. Lett.* **815**, L12 (2015).
71. Johnstone, C. P., Güdel, M., Brott, I. & Lüftinger, T. Stellar winds on the main-sequence. II. The evolution of rotation and winds. *Astron. Astrophys.* **577**, A28 (2015).
72. O'Rourke, J. G., Gillmann, C. & Tackley, P. Prospects for an ancient dynamo and modern crustal remanent magnetism on Venus. *Earth Planet. Sci. Lett.* **502**, 46–56 (2018).
73. Jacobson, S. A., Rubie, D. C., Hernlund, J., Morbidelli, A. & Nakajima, M. Formation, stratification, and mixing of the cores of Earth and Venus. *Earth Planet. Sci. Lett.* **474**, 375–386 (2017).
74. Gunell, H. et al. Why an intrinsic magnetic field does not protect a planet against atmospheric escape. *Astron. Astrophys.* **614**, L3 (2018).
75. Pieters, C. M. et al. The color of the surface of Venus. *Science* **234**, 1379–1383 (1986).
76. Masset, F. & Snellgrove, M. Reversing type II migration: resonance trapping of a lighter giant protoplanet. *Mon. Not. R. Astron. Soc.* **320**, 55–59 (2001).
77. Morbidelli, A. & Crida, A. The dynamics of Jupiter and Saturn in the gaseous protoplanetary disk. *Icarus* **191**, 158–171 (2007).
78. Pierens, A., Raymond, S. N., Nesvorny, D. & Morbidelli, A. Outward migration of Jupiter and Saturn in 3:2 or 2:1 resonance in radiative disks: implications for the Grand Tack and Nice models. *Astrophys. J.* **795**, L11 (2014).
79. Raymond, S. N., O'Brien, D. P., Morbidelli, A. & Kaib, N. A. Building the terrestrial planets: constrained accretion in the inner Solar System. *Icarus* **203**, 644–662 (2009).
80. Walsh, K. J., Morbidelli, A., Raymond, S. N., O'Brien, D. P. & Mandell, A. M. A low mass for Mars from Jupiter's early gas-driven migration. *Nature* **475**, 206 (2011).
81. Bottke, W. F. et al. Stochastic late accretion to Earth, the Moon, and Mars. *Science* **330**, 1527–1530 (2010).
82. Walker, R. J. Highly siderophile elements in the Earth, Moon and Mars: update and implications for planetary accretion and differentiation. *Chem. Erde* **69**, 101–125 (2009).
83. Morbidelli, A. et al. The timeline of the lunar bombardment: revisited. *Icarus* **305**, 262–276 (2018).
84. Touboul, M., Kleine, T., Bourdon, B., Palme, H. & Wieler, R. Late formation and prolonged differentiation of the Moon inferred from W isotopes in lunar metals. *Nature* **450**, 1206–1209 (2007).
85. Kleine, T. et al. Hf–W chronology of the accretion and early evolution of asteroids and terrestrial planets. *Geochim. Cosmochim. Acta* **73**, 5150–5188 (2009).
86. Grady, M. M. & Wright, I. P. Elemental and isotopic abundances of carbon and nitrogen in meteorites. *Space Sci. Rev.* **106**, 231–248 (2003).
87. Schaefer, L. & Fegley, B. Jr Outgassing of ordinary chondritic material and some of its implications for the chemistry of asteroids, planets, and satellites. *Icarus* **186**, 462–483 (2007).
88. Schaefer, L. & Fegley, B. Jr Redox states of initial atmospheres outgassed on rocky planets and planetesimals. *Astrophys. J.* **843**, 120 (2017).
89. Brasser, R., Mojzsis, S. J., Matsumura, S. & Ida, S. The cool and distant formation of Mars. *Earth Planet. Sci. Lett.* **468**, 85–93 (2017).
90. Vickery, A. M. & Melosh, H. J. in *Global Catastrophes in Earth History* (eds Sharpton, V. L. & Ward, P. D.) 289–300 (GSA Special Papers Vol. 247, Geological Society of America, 1990).
91. Shuvalov, V. Atmospheric erosion induced by oblique impacts. In *41st Lunar Planetary Science Conference* Abstract 1191 (Lunar and Planetary Institute, 2010).
92. Shuvalov, V., Kührt, E., de Niem, D. & Wünnemann, K. Impact induced erosion of hot and dense atmospheres. *Planet. Space Sci.* **98**, 120–127 (2014).
93. Genda, H. & Abe, Y. Survival of a proto-atmosphere through the stage of giant impacts: the mechanical aspects. *Icarus* **164**, 149–162 (2003).
94. Svetsov, V. V. & Shuvalov, V. V. Silicate impact-vapor condensate on the Moon: theoretical estimates versus geochemical data. *Geochim. Cosmochim. Acta* **173**, 50–63 (2016).
95. Pham, L. B. S., Karatekin, Ö. & Dehant, V. Effects of impacts on the atmospheric evolution: comparison between Mars, Earth, and Venus. *Planet. Space Sci.* **59**, 1087–1092 (2011).
96. Pham, L. B. S. & Karatekin, Ö. Scenarios of atmospheric mass evolution on Mars influenced by asteroid and comet impacts since the late Noachian. *Planet. Space Sci.* **125**, 1–11 (2016).
97. Abramov, O. & Mojzsis, S. J. Microbial habitability of the Hadean earth during the late heavy bombardment. *Nature* **459**, 419–422 (2009).
98. Ruedas, T. & Breuer, D. Dynamical effects of multiple impacts: impacts on a Mars-like planet. *Phys. Earth Planet. Inter.* **287**, 76–92 (2019).

Acknowledgements

We thank F. Crameri for providing the perceptually uniform colour map used in Fig. 4[51]. We thank D. Rubie for his comments. We also thank R. Brasser and K. Zahnle. C.G., V. Dehant and V. Debaille were supported by BELSPO PlanetTOPERS IUAP programme and ET-HoME Excellence of Science programme. V. Debaille thanks the FRS-FNRS and ERC StG ISoSyC FP7/336718. M.S. acknowledges the National Center for Competence in Research 'PlanetS' supported by the Swiss National Science Foundation (SNSF). V. Dehant was financially supported by the Belgian PRODEX program managed by the European Space Agency in collaboration with the Belgian Federal Science Policy Office.

Author contributions

C.G. wrote the atmosphere, outgassing and escape codes, and designed the coupling between models. C.G. and G.J.G. wrote the impact code. P.J.T. wrote the StagYY code. S.N.R. designed the N-body models and designed related simulations. C.G. and G.J.G. designed the set of StagYY simulations. C.G. ran all the simulations. All the authors discussed the results and contributed to the manuscript.

Competing interests

The authors declare no competing interests.

Additional information

Extended data is available for this paper at https://doi.org/10.1038/s41561-020-0561-x.

Supplementary information is available for this paper at https://doi.org/10.1038/s41561-020-0561-x.

Correspondence and requests for materials should be addressed to C.G.

Peer review information Primary Handling Editor: Stefan Lachowycz.

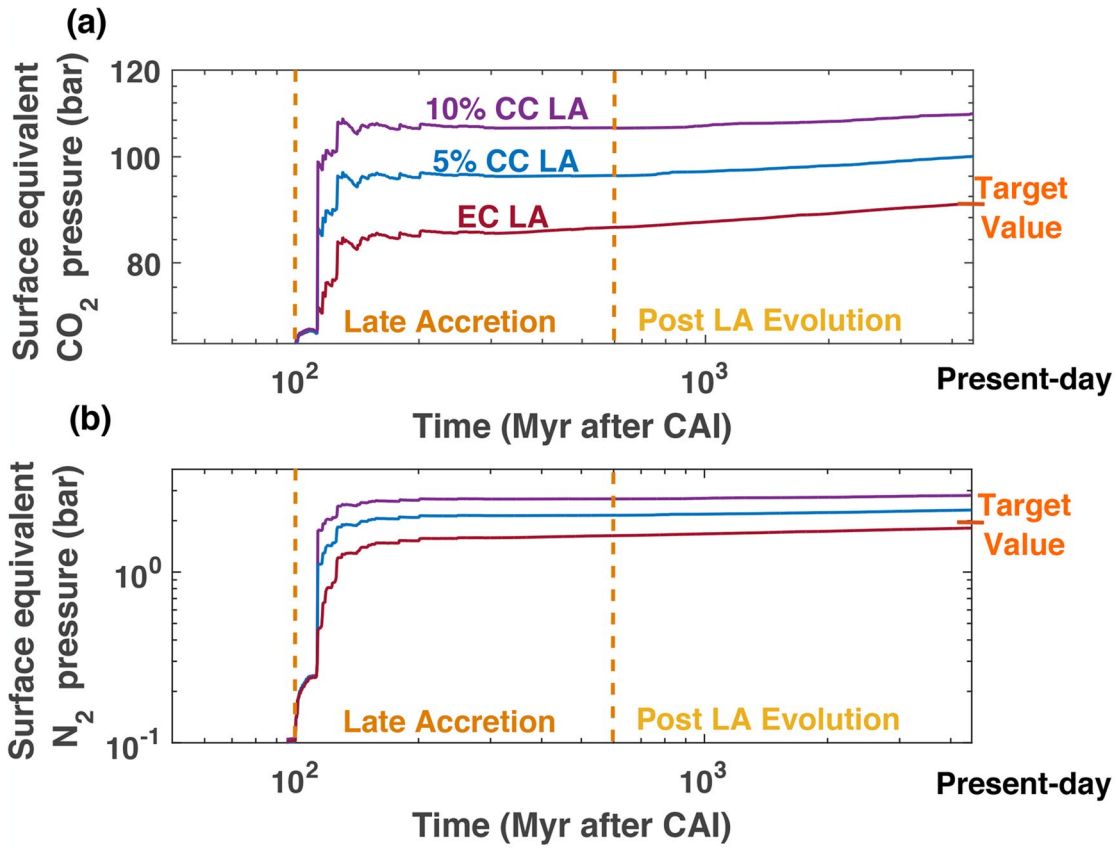

Extended Data Fig. 1 | Evolution of CO_2 and N_2 pressure. Time evolution of **a**, CO_2 and **b**, N_2 abundances in the Venus atmosphere for three different LA compositions, labelled as CC material percentage of the total LA mass delivery. MAX parameters and LA scenario D starting at 100 Myr after CAI formation are used.

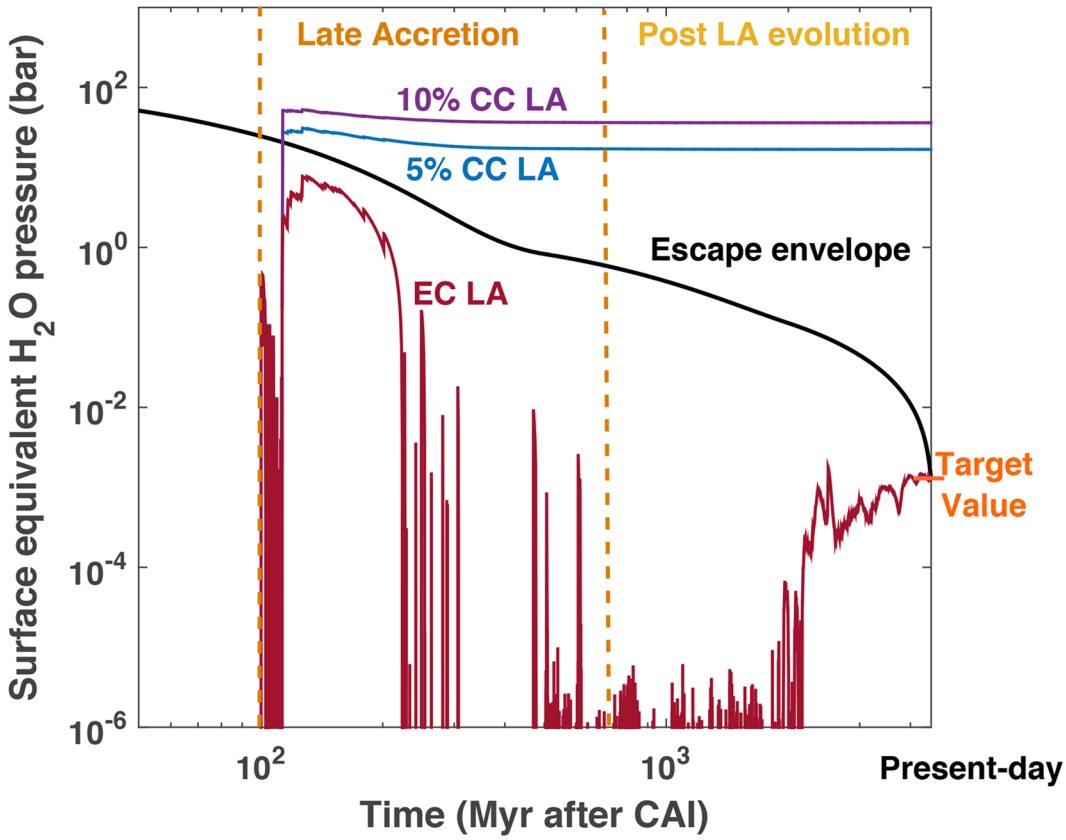

Extended Data Fig. 2 | Evolution of water in the atmosphere of Venus. Time evolution of H_2O in the Venus atmosphere for MED conditions assuming different LA compositions, labelled as CC material percentage of the total LA mass delivery. LA scenario D starting at 100 Myr after CAI formation is used.

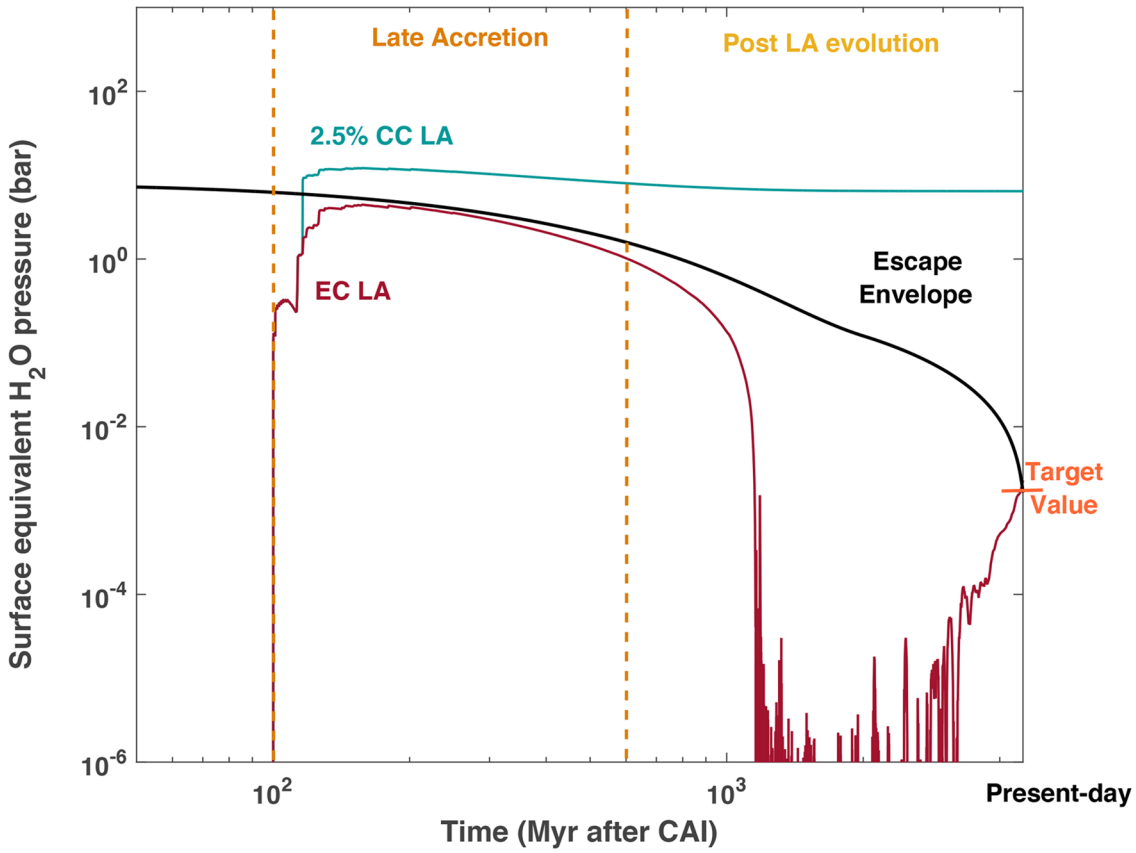

Extended Data Fig. 3 | Evolution of water in the atmosphere of Venus. Time evolution of H_2O in the Venus atmosphere for MIN conditions assuming different LA compositions, labelled as CC material percentage of the total LA mass delivery. LA scenario D starting at 100 Myr after CAI formation is used.

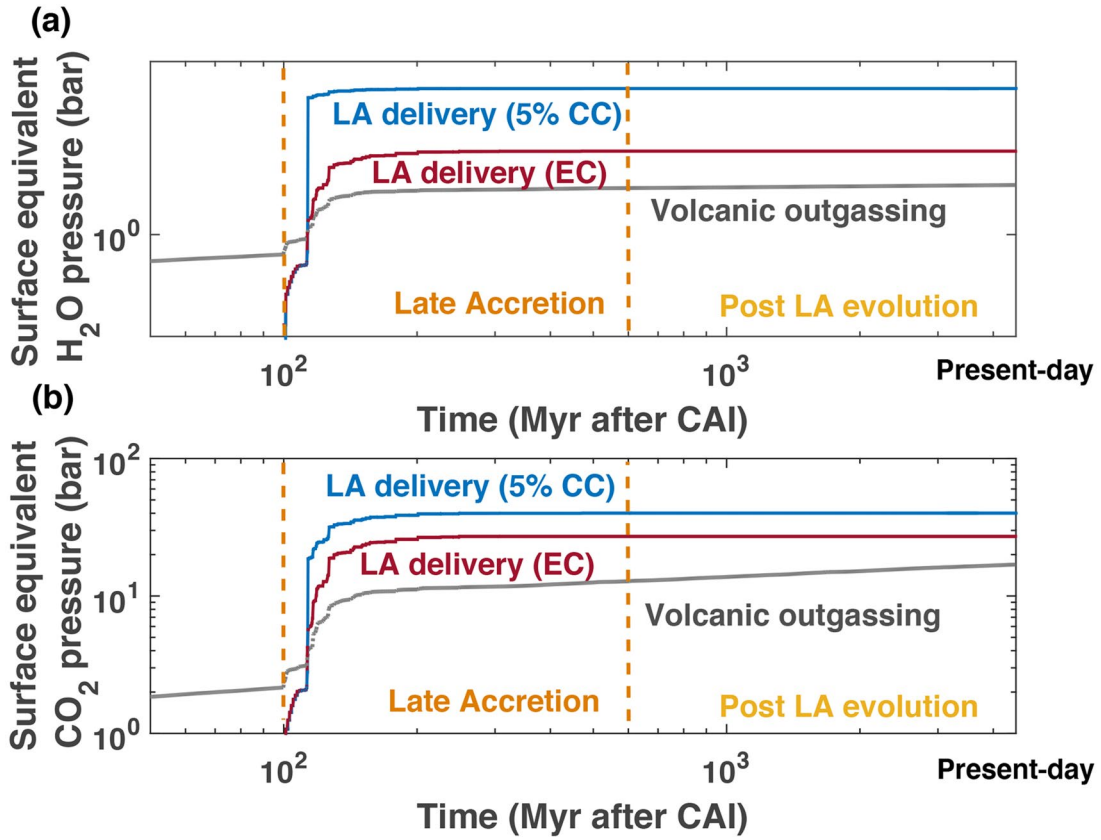

Extended Data Fig. 4 | Comparison of delivery mechanisms. Volcanic and impact sources for **a**, H_20 and **b**, CO_2. All shown cases employ MAX parameters and LA scenario D starting at 100 Myr after CAIs.

Parameter name	Parameter value
Mantle convection modeling	
Planetary radius	6052 km
Planetary mass	4.8673×10^{24} kg
CMB radius	3110 km
Mantle depth	2942 km
Surface gravity	8.87 m/s^2
Surface temperature (for uncoupled cases)	740 K
Initial CMB temperature	4025 K
Specific heat capacity	1200 J/kg/K
Latent heat of silicate melting	600 kJ/kg
Reference viscosity	10^{20} Pa s
Friction coefficient	0.5
Surface yield stress	100 MPa
Internal heating at present-day	5.2×10^{-12} W/kg
Internal heating rate at model start	18.77×10^{-12} W/kg
Half-life time of radiogenic heating	2.43 Gyr
Volcanic outgassing modeling	
Volatiles eruption coefficient	10%
H_2O concentration (initial ; present-day)	80 ppm; 20 ppm
CO_2 concentration (initial ; present-day)	400 ppm; 100 ppm
N_2 concentration (initial ; present-day)	20 ppm; 5 ppm
Maximum eruption depth	300 km
Atmosphere and escape modeling	
Solar irradiance (present-day)	2613.9 W/m^2
Initial CO_2 pressure (post magma ocean)	65 bar
Initial H_2O pressure (post magma ocean)	0 bar
Initial N_2 pressure (post magma ocean)	0 bar
Equilibrium temperature (present-day)	232 K
Reference oxygen escape rate (non-thermal; present-day)	6.0×10^{25} s^{-1}
Base of the exosphere	200 km
Radius of the extended atmosphere (in planetary radii)	8
Energy deposition efficiency (hydrodynamic escape)	15%
Exospheric temperature (hydrodynamic escape)	2000 K
Impact modeling	
Efficiency of impact energy transfer into mantle	0.3
Impactor density	2700 kg/m^3
EC H_2O content	0.1%
EC CO_2 content	0.4%
EC N_2 content	0.02%
CC H_2O content	8%
CC CO_2 content	4%
CC N_2 content	0.2%

Extended Data Fig. 5 | List of parameters and values.

Parameter	MAX	MED	MIN
Oxygen escape scheme (from Kulikov et al., 2006)	Case 2b	Case 2b	Case 4
Multiplication factor for all mechanisms	5	2.5	6
Impact erosion scheme	Tangent plane	Tangent plane	SOVA models

Extended Data Fig. 6 | MAX, MED and MIN specific parameter sets.